Geochemical Perspectives Letters

No V-Fe-Zn isotopic variation in basalts from the 2021 Fagradalsfjall eruption

M.A. Stow[1*,†], J. Prytulak[1], K.W. Burton[1], G.M. Nowell[1], E.W. Marshall[2], S.A. Halldórsson[2], S. Matthews[2,3], M.B. Rasmussen[2,‡], E. Ranta[2,§], A. Caracciolo[2]

https://doi.org/10.7185/geochemlet.2335

Abstract

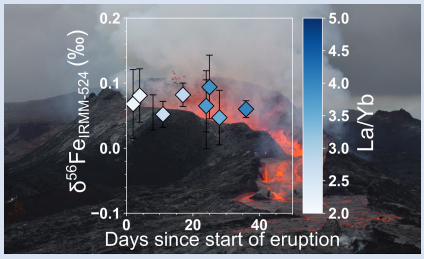

The Earth's mantle is chemically heterogeneous in space and time, which is often reflected by variable isotopic compositions of mantle derived basalts. Basalts from the first 40 days of the 2021 Fagradalsfjall eruption, Reykjanes Peninsula, Iceland, display systematic temporal variations in the ratios of incompatible elements alongside resolvable variations in Sr, Nd and Pb radiogenic isotopes. These variations reflect progressive influx of magma derived from melting of a deeper, more enriched and potentially lithologically distinct source. We use this eruptive time series to conduct the first combined V-Fe-Zn isotope study, exploring the sensitivity of the combined isotopic approach, with particular focus on fingerprinting source lithological heterogeneity. We find no analytically resolvable change in V ($\delta^{51}V_{AA}$ between -0.95 ± 0.09 ‰ 2 s.d. and -0.86 ± 0.07 ‰ 2 s.d.), Fe ($\delta^{56}Fe_{IRMM\text{-}524}$ between $+0.047 \pm 0.042$ ‰ 2 s.d. and $+0.094 \pm 0.049$ ‰ 2 s.d.) and Zn ($\delta^{66}Zn_{AA\text{-}ETH}$ between -0.042 ± 0.003 ‰ 2 s.d. and $+0.013 \pm 0.027$ ‰ 2 s.d.) isotopic compositions. The lack of variability in V-Fe-Zn isotopes, despite the evolving trace element and radiogenic isotope ratios, suggests there is no significant contribution of melts from a lithologically distinct (pyroxenite) mantle component under the Reykjanes Peninsula.

Received 30 June 2023 | Accepted 26 September 2023 | Published 30 October 2023

Introduction

It is widely accepted that crustal recycling has led to the formation of a chemically and isotopically heterogeneous upper mantle. Due to the relative inaccessibility of the mantle reservoir, most information about its composition comes from the study of mantle-derived basalts. Variations in the major, trace element and radiogenic isotopic composition of basalts require the presence of chemically enriched and depleted mantle domains (*e.g.*, Hofmann, 1997). Enriched components can exist as pyroxene-rich (pyroxenite/eclogite) lithologies derived from subducted oceanic crust, which are more fusible and melt at a lower solidus temperature than peridotite (*e.g.*, Pertermann and Hirschmann, 2003). Therefore, minor pyroxenite melting can dominate the trace element signature of basalts, making investigation of the spatial extent and characteristics of these heterogeneities challenging.

An emerging approach for investigating potential variation in mantle lithology is to use transition metal stable isotopes (TMI), the most well studied being Fe (*e.g.*, Williams and Bizimis, 2014; Konter *et al.*, 2016; Soderman *et al.*, 2021). At equilibrium, stable isotope fractionation between phases is theoretically controlled by bond strength, with heavier isotopes concentrating in stronger bonds where elements are present in higher oxidation state and lower bond coordination (*e.g.*, Schauble, 2004). Analytically resolvable variations in the magnitude of TMI equilibrium mineral-mineral and mineral-melt isotopic fractionation at magmatic temperatures have been both theoretically predicted and directly documented (*e.g.*, Prytulak *et al.*, 2017; Sossi and O'Neill, 2017; Stow *et al.*, 2022). For example, in the case of Fe, the difference in bonding environment and valence between pyroxene and olivine leads to heavier Fe isotopic composition in pyroxene-rich lithologies derived from subducted oceanic crust compared to olivine-rich peridotite (*e.g.*, Williams and Bizimis, 2014). Thus, the transition metal stable isotopic composition of primitive basalts is an attractive prospect for fingerprinting magmatic source lithology.

Although TMI could theoretically track variations in mantle lithology, there is debate about their efficacy. Whether signals of mantle heterogeneity are preserved in primitive basalts depends on the contrast in isotopic composition between the different mantle sources and the proportions of each source melted (*e.g.*, Soderman *et al.*, 2022).

The 2021 Fagradalsfjall eruption on the Reykjanes Peninsula, Iceland, provides a unique opportunity to investigate

1. Department of Earth Sciences, Durham University, Durham, UK
2. Nordic Volcanological Center, Institute of Earth Sciences, University of Iceland, Reykjavík, Iceland
3. Department of Earth Sciences, University of Cambridge, Cambridge, UK
† Current Address: Department of Earth Sciences, University of Oxford, Oxford, UK
‡ Current Address: Department of Geosciences and Natural Resource Management, University of Copenhagen, Copenhagen, Denmark
§ Current Address: Department of Geosciences and Geography, University of Helsinki, Helsinki, Finland
* Corresponding author (Email: madeleine.stow@earth.ox.ac.uk)

the relationship between potential mantle lithological heterogeneity and the transition metal stable isotope composition of basalts. Continuous eruption and high-resolution sampling of basaltic material occurred from 19 March to 18 September 2021. The Fagradalsfjall time series is an ideal sample set for several reasons:

1. It is generally accepted that the mantle beneath Iceland, and the Reykjanes peninsula specifically, is lithologically heterogeneous and contains various depleted and enriched domains (*e.g.*, Maclennan, 2008; Shorttle and Maclennan, 2011; Rasmussen *et al.*, 2020; Harðardóttir *et al.*, 2022).
2. The Fagradalsfjall basalts display systematic temporal variations in trace element compositions over the first 40 days of the eruption, which requires the melting of chemically, and potentially lithologically, distinct sources (Bindeman *et al.*, 2022; Halldórsson *et al.*, 2022). Increases in La/Yb and K_2O/TiO_2 suggest recharge of melts derived from a more enriched source during the eruption, consistent with increasing $^{206}Pb/^{204}Pb$ and $^{87}Sr/^{86}Sr$, and decreasing $^{143}Nd/^{144}Nd$ (Halldórsson *et al.*, 2022).
3. The basalts have high MgO content (8.8–10 wt. %) and show no evidence for crustal assimilation or long-term crustal storage (Bindeman *et al.*, 2022; Halldórsson *et al.*, 2022; Kahl *et al.*, 2023). Therefore, the geochemical variability of these primitive basalts most likely reflects variation in the mantle source.

This work provides the first combined V, Fe and Zn stable isotope investigation of mantle-derived basalts. Iron, V and Zn are concentrated in different mineral phases with distinct equilibrium mineral-melt fractionation factors controlled by mineral bonding environment. Therefore, Fe, V and Zn should have distinctive responses to variations in mantle lithology. It follows that the combination of the three systems likely provides better constraint than any one system in isolation. Iron isotopes have been used to infer the presence of pyroxene-rich domains in mantle sources (*e.g.*, Williams and Bizimis, 2014; Konter *et al.*, 2016; Nebel *et al.*, 2019; Soderman *et al.*, 2021). The influence of lithological heterogeneity on V isotopes is less well constrained; however, several studies report V isotopic compositions of Icelandic lavas, which can be compared to the Fagradalsfjall data (Prytulak *et al.*, 2013, 2017; Novella *et al.*, 2020). It is debated whether Zn isotopes are fractionated during partial melting of distinct lithologies (*e.g.*, Doucet *et al.*, 2016; Day *et al.*, 2022), or if variation is largely controlled by kinetic fractionation during melt or fluid percolation (Huang *et al.*, 2019; Fang *et al.*, 2022). Finally, Fe and V are redox sensitive elements whereas Zn is a monovalent element in terrestrial systems. Consequently, potential redox variations will not directly influence Zn isotopic fractionation, but may influence Fe and V (*e.g.*, Stow *et al.*, 2022). Thus, a multi-isotope approach can address existing uncertainties by evaluating the relationships between the three isotope systems. The Fagradalsfjall basalts and their well-characterised secular chemical variations provide an opportunity to evaluate the sensitivity of V-Fe-Zn variations to potential changes in parameters such as oxygen fugacity, partial melting, and lithological heterogeneity.

Methods

We determined the V, Fe and Zn stable isotopic compositions of 10 glassy basalts erupted between 21 March and 24 April 2021, which capture the full breadth of trace element variability during the overall eruption. These are newly prepared aliquots of the same samples analysed by Halldórsson *et al.* (2022). Chemical separation and isotope ratio measurements were carried out in the Arthur Holmes Isotope Geology Laboratory, Durham University. The column chromatography procedure quantitatively separated V, Fe and Zn from the same sample digestion. See the Supplementary Information for a full description of the methods. Analytical uncertainties, reported as 2 s.d., are typically <0.1 ‰ for $\delta^{51}V$, <0.05 ‰ for $\delta^{56}Fe$ and <0.03 ‰ for $\delta^{66}Zn$ (see Table S-1).

Results and Discussion

The first order observation of this study is that there is no analytically resolvable temporal variation in V, Fe or Zn isotopic compositions of the Fagradalsfjall basalts over the first 40 days of the eruption (Fig. 1; Table S-1). There are limited published Icelandic V-Fe-Zn data for comparison, but the basalts have similar isotopic compositions to mafic samples (<50 wt. % whole rock SiO_2) from Hekla volcano (grey bars in Fig. 1;

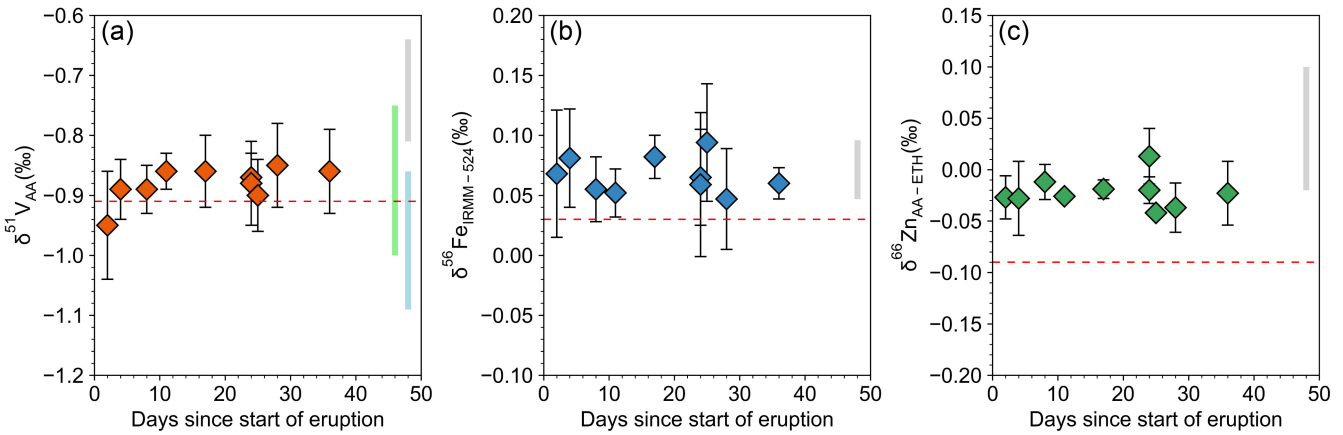

Figure 1 **(a)** Vanadium, **(b)** iron and **(c)** zinc isotopic compositions over the first 40 days of the eruption. Error bars are 2 s.d. of at least three measurements of each sample. Red dashed lines show estimates of the Bulk Silicate Earth (BSE); $\delta^{51}V_{AA} = -0.91 \pm 0.09$ ‰ (Qi *et al.*, 2019), $\delta^{56}Fe_{IRMM\text{-}524} = +0.030 \pm 0.007$ ‰ (Sossi *et al.*, 2016) and $\delta^{66}Zn_{AA\text{-}ETH} = -0.09 \pm 0.08$ ‰ (Fang *et al.*, 2022). Grey vertical bands indicate the ranges of V (Prytulak *et al.*, 2017), Fe (Schuessler *et al.*, 2009) and Zn (Chen *et al.*, 2013) isotopic compositions in lavas from Hekla volcano with whole rock $SiO_2 < 50$ wt. %. Vertical blue and green bars indicate the ranges of V isotopic compositions in basalts from the Reykjanes Ridge (Novella *et al.*, 2020) and Reykjanes Peninsula (Prytulak *et al.*, 2013).

Schuessler *et al.*, 2009; Chen *et al.*, 2013; Prytulak *et al.*, 2017). In addition, $\delta^{51}V$ values are within error of basalts from the Reykjanes Ridge (blue bar in Fig. 1a; Novella *et al.*, 2020) and Reykjanes Peninsula (green bar in Fig. 1a; Prytulak *et al.*, 2013).

The Fagradalsfjall basalts display a greater variation in major and trace element compositions over the first 40 days of the eruption than have been observed in historical lavas from the Reykjanes Peninsula (Halldórsson *et al.*, 2022). Bindeman *et al.* (2022) and Halldórsson *et al.* (2022) proposed similar models to explain these geochemical variations. A depleted melt sourced from shallow mantle melting is thought to dominate the initial eruptive products. Enriched melts derived from deeper and lower degrees of mantle melting became more significant as the eruption proceeded. Rapid mixing of depleted and enriched melts occurs in the deep magma reservoir which feeds the eruption, generating the linear trends observed in the trace elements (Halldórsson *et al.*, 2022). However, there is no correlation between V-Fe-Zn isotopes and K_2O/TiO_2 or La/Yb (Fig. 2), the parameters used to demonstrate progressive contribution of melts derived from a deeper and/or more enriched source (Halldórsson *et al.*, 2022).

The Fagradalsfjall basalts also record resolvable variation in Sr, Nd and Pb isotopic compositions over the first 40 days of the eruption, which are likewise thought to reflect the presence of melts from distinct mantle sources (Halldórsson *et al.*, 2022). There is also no correlation between V-Fe-Zn isotopes and Sr, Nd or Pb isotopes (Figs. 2, S-4).

Although there is no variation in V-Fe-Zn isotopes at Fagradalsfjall, several previous studies of ocean island basalts have observed correlations between $\delta^{56}Fe$ and the ratios of trace elements and radiogenic isotopes. These studies suggest that heavy Fe isotope signatures are at least in part inherited from an isotopically heavy pyroxene-bearing source (*e.g.*, Konter *et al.*, 2016; Nebel *et al.*, 2019; Soderman *et al.*, 2021; Shi *et al.*, 2022). However, these studies often analyse samples erupted from multiple volcanic vents across different islands, and are therefore not directly comparable to the Fagradalsfjall eruption. To facilitate a more direct comparison, we plot a selection of the literature

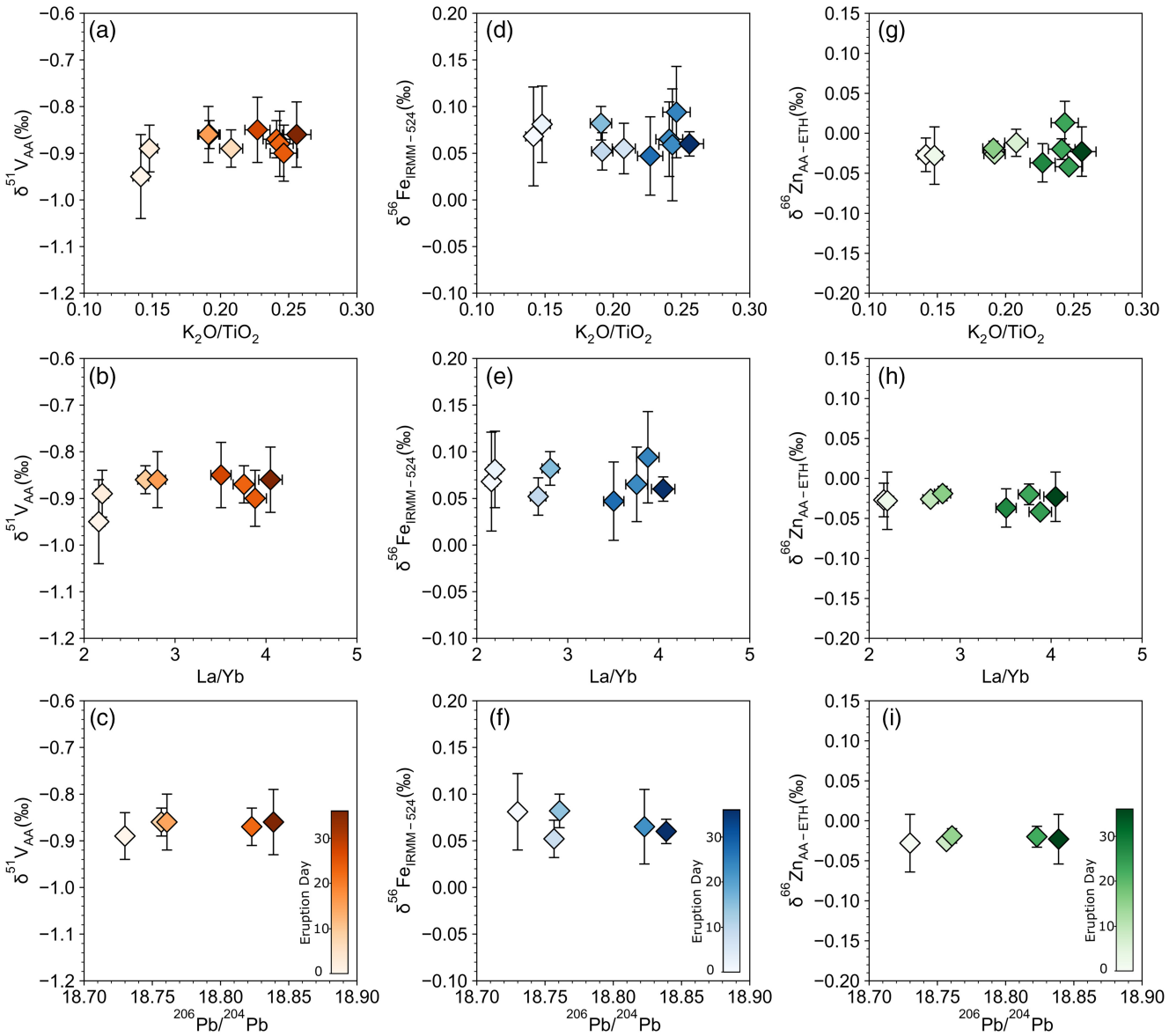

Figure 2 **(a–c)** Vanadium, **(d–f)** iron and **(g–i)** zinc isotopic compositions against whole rock **(a, d, g)** K_2O/TiO_2, **(b, e, h)** La/Yb and **(c, f, i)** $^{206}Pb/^{204}Pb$ from Halldórsson *et al.* (2022). The more enriched melts have higher La/Yb, K_2O/TiO_2 and $^{206}Pb/^{204}Pb$. The colour bar indicates the day the sample was erupted. Plots of isotopic composition against Sr and Nd isotopes are shown in Figure S-4.

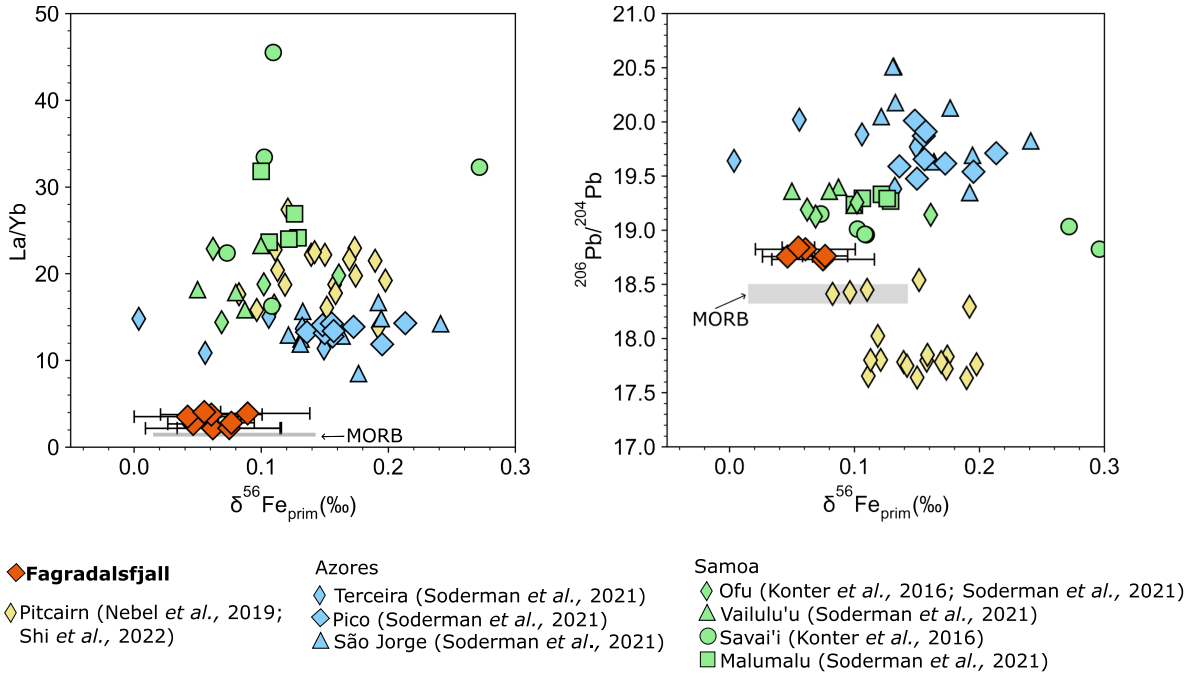

Figure 3 Iron isotopic compositions of selected ocean island basalts from the literature. The $\delta^{56}Fe_{prim}$ values are calculated as described in the Supplementary Information. The MORB La/Yb and $^{206}Pb/^{204}Pb$ values are from Gale *et al.* (2013), and MORB $\delta^{56}Fe_{prim}$ values from Sossi *et al.* (2016).

data where at least four samples are from the same volcanic island, and where the presence of a pyroxene-bearing source has been proposed (Fig. 3). Although the Fagradalsfjall basalts do display resolvable variations in trace element and radiogenic isotope ratios, these ranges are much smaller than those observed in the other ocean island basalts. It is perhaps not surprising that the Fagradalsfjall basalts display no change in Fe isotopic composition. Although minor amounts of pyroxenite are required to explain some of the changes in the trace element and radiogenic isotope compositions of the basalts (*i.e.* <10–20 % pyroxenite melt; see Supplementary Information), this amount would be insufficient to drive changes in basalt $\delta^{56}Fe$. A binary mixing model (Fig. S-3) demonstrates that a contribution of at least 40–50 % enriched melt with $\delta^{56}Fe > 0.2$ ‰ is generally required to generate resolvable Fe isotopic variation. Therefore, the lack of variation in $\delta^{56}Fe$ in the Fagradalsfjall basalts is consistent with the lack of a volumetrically significant contribution of melts from a lithologically distinct source with a heavy Fe isotopic composition.

The controls on V and Zn isotope fractionation during mantle melting are not as well constrained as for Fe, but we can examine covariations between the three systems to investigate the drivers of isotopic fractionation. Previous empirical and modelling studies have suggested that V isotopes are insensitive to the presence of pyroxenite lithologies (Novella *et al.*, 2020; Soderman *et al.*, 2022). The lack of correlation between $\delta^{56}Fe$ and $\delta^{51}V$ in the Fagradalsfjall basalts supports this inference. In addition, the lack of correlation between these two redox sensitive elements suggests that there is no variation in mantle oxygen fugacity.

Previous studies suggest that Zn isotopic variability may be controlled by kinetic fractionation during percolation of melts and/or fluids through the mantle, and consequently hybridised mantle should have more variable $\delta^{66}Zn$ than peridotites (Huang *et al.*, 2019; Fang *et al.*, 2022). Therefore, the lack of covariation between Fe and Zn isotopes in the Fagradalsfjall basalts also supports the lack of a volumetrically significant contribution of melts from an enriched source.

This work has explored the sensitivity of a novel combination of three isotope systems (V, Fe and Zn) with contrasting chemical behaviours. In the case of the Fagradalsfjall high resolution eruptive time series, the lack of V-Fe-Zn isotopic variation suggests that there is no significant contribution of melts from a pyroxenite source. However, a multi-isotope approach still holds promise in identifying and disentangling processes and components involved in the generation of mantle-derived basalts.

Acknowledgements

MAS was supported by a NERC IAPETUS Doctoral Training Programme (NE/L002590/1) studentship. EWM, SAH, SM, AC, MBR and ER were supported by the Icelandic Research Fund, grant number 228933-051 and by the Department of Civil Protection and Emergency Management. This work was greatly improved by detailed reviews from M. Bizimis and an anonymous reviewer, and the comments and efficient editorial handling of R. Fonseca.

Editor: Raúl Fonseca

Data Access Statement

All data generated during this study are included in the published article and the Supplementary Information.

Additional Information

Supplementary Information accompanies this letter at https://www.geochemicalperspectivesletters.org/article2335.

Cite this letter as: Stow, M.A., Prytulak, J., Burton, K.W., Nowell, G.M., Marshall, E.W., Halldórsson, S.A., Matthews, S., Rasmussen, M.B., Ranta, E., Caracciolo, A. (2023) No V-Fe-Zn isotopic variation in basalts from the 2021 Fagradalsfjall eruption. *Geochem. Persp. Let.* 27, 54–58. https://doi.org/10.7185/geochemlet.2335

References

Bindeman, I.N., Deegan, F.M., Troll, V.R., Thordarson, T., Höskuldsson, Á., Moreland, W.M., Zorn, E.U., Shevchenko, A.V., Walter, T.R. (2022) Diverse mantle components with invariant oxygen isotopes in the 2021 Fagradalsfjall eruption, Iceland. *Nature Communications* 13, 3737. https://doi.org/10.1038/s41467-022-31348-7

Chen, H., Savage, P.S., Teng, F.-Z., Helz, R.T., Moynier, F. (2013) Zinc isotope fractionation during magmatic differentiation and the isotopic composition of the bulk Earth. *Earth and Planetary Science Letters* 369–370, 34–42. https://doi.org/10.1016/j.epsl.2013.02.037

Day, J.M.D., Moynier, F., Ishizuka, O. (2022) A partial melting control on the Zn isotope composition of basalts. *Geochemical Perspectives Letters* 23, 11–16. https://doi.org/10.7185/geochemlet.2230

Doucet, L.S., Mattielli, N., Ionov, D.A., Debouge, W., Golovin, A.V. (2016) Zn isotopic heterogeneity in the mantle: A melting control? *Earth and Planetary Science Letters* 451, 232–240. https://doi.org/10.1016/j.epsl.2016.06.040

Fang, S.-B., Huang, J., Zhang, X.-C., Ionov, D.A., Zhao, Z.-F., Huang, F. (2022) Zinc isotope fractionation in mantle rocks and minerals, and a revised δ^{66}Zn value for the Bulk Silicate Earth. *Geochimica et Cosmochimica Acta* 338, 79–92. https://doi.org/10.1016/j.gca.2022.10.017

Gale, A., Dalton, C.A., Langmuir, C.H., Su, Y., Schilling, J.-G. (2013) The mean composition of ocean ridge basalts. *Geochemistry, Geophysics, Geosystems* 14, 489–518. https://doi.org/10.1029/2012GC004334

Halldórsson, S.A., Marshall, E.W., Caracciolo, A., Matthews, S., Bali, E., Rasmussen, M.B., Ranta, E., Robin, J.G., Guðfinnsson, G.H., Sigmarsson, O., Maclennan, J., Jackson, M.G., Whitehouse, M.J., Jeon, H., van der Meer, Q.H.A., Mibei, G.K., Kalliokoski, M.H., Repczynska, M.M., Rúnarsdóttir, R.H., Sigurðsson, G., Pfeffer, M.A., Scott, S.W., Kjartansdóttir, R., Kleine, B.I., Oppenheimer, C., Aiuppa, A., Ilyinskaya, E., Bitetto, M., Giudice, G., Stefánsson, A. (2022) Rapid shifting of a deep magmatic source at Fagradalsfjall volcano, Iceland. *Nature* 609, 529–534. https://doi.org/10.1038/s41586-022-04981-x

Harðardóttir, S., Matthews, S., Halldórsson, S.A., Jackson, M.G. (2022) Spatial distribution and geochemical characterization of Icelandic mantle end-members: Implications for plume geometry and melting processes. *Chemical Geology* 604, 120930. https://doi.org/10.1016/j.chemgeo.2022.120930

Hofmann, A.W. (1997) Mantle geochemistry: the message from oceanic volcanism. *Nature* 385, 219–229. https://doi.org/10.1038/385219a0

Huang, J., Ackerman, L., Zhang, X.-C., Huang, F. (2019) Mantle Zn Isotopic Heterogeneity Caused by Melt-Rock Reaction: Evidence From Fe-Rich Peridotites and Pyroxenites From the Bohemian Massif, Central Europe. *Journal of Geophysical Research: Solid Earth* 124, 3588–3604. https://doi.org/10.1029/2018JB017125

Kahl, M., Mutch, E.J.F., Maclennan, J., Morgan, D.J., Couperthwaite, F., Bali, E., Thordarson, T., Guðfinnsson, G.H., Walshaw, R., Buisman, I., Buhre, S., van der Meer, Q.H.A., Caracciolo, A., Marshall, E.W., Rasmussen, M.B., Gallagher, C.R., Moreland, W.M., Höskuldsson, A., Askew, R.A. (2023) Deep magma mobilization years before the 2021 CE Fagradalsfjall eruption, Iceland. *Geology* 51, 184–188. https://doi.org/10.1130/G50340.1

Konter, J.G., Pietruszka, A.J., Hanan, B.B., Finlayson, V.A., Craddock, P.R., Jackson, M.G., Dauphas, N. (2016) Unusual δ^{56}Fe values in Samoan rejuvenated lavas generated in the mantle. *Earth and Planetary Science Letters* 450, 221–232. https://doi.org/10.1016/j.epsl.2016.06.029

Maclennan, J. (2008) Lead isotope variability in olivine-hosted melt inclusions from Iceland. *Geochimica et Cosmochimica Acta* 72, 4159–4176. https://doi.org/10.1016/j.gca.2008.05.034

Nebel, O., Sossi, P.A., Bénard, A., Arculus, R.J., Yaxley, G.M., Woodhead, J.D., Davies, D.R., Ruttor, S. (2019) Reconciling petrological and isotopic mixing mechanisms in the Pitcairn mantle plume using stable Fe isotopes. *Earth and Planetary Science Letters* 521, 60–67. https://doi.org/10.1016/j.epsl.2019.05.037

Novella, D., Maclennan, J., Shorttle, O., Prytulak, J., Murton, B.J. (2020) A multi-proxy investigation of mantle oxygen fugacity along the Reykjanes Ridge. *Earth and Planetary Science Letters* 531, 115973. https://doi.org/10.1016/j.epsl.2019.115973

Pertermann, M., Hirschmann, M.M. (2003) Partial melting experiments on a MORB-like pyroxenite between 2 and 3 GPa: Constraints on the presence of pyroxenite in basalt source regions from solidus location and melting rate. *Journal of Geophysical Research: Solid Earth* 108, 2125. https://doi.org/10.1029/2000JB000118

Prytulak, J., Nielsen, S.G., Ionov, D.A., Halliday, A.N., Harvey, J., Kelley, K.A., Niu, Y.L., Peate, D.W., Shimizu, K., Sims, K.W.W. (2013) The stable vanadium isotope composition of the mantle and mafic lavas. *Earth and Planetary Science Letters* 365, 177–189. https://doi.org/10.1016/j.epsl.2013.01.010

Prytulak, J., Sossi, P.A., Halliday, A.N., Plank, T., Savage, P.S., Woodhead, J.D. (2017) Stable vanadium isotopes as a redox proxy in magmatic systems? *Geochemical Perspectives Letters* 3, 75–84. https://doi.org/10.7185/geochemlet.1708

Qi, Y.-H., Wu, F., Ionov, D.A., Puchtel, I.S., Carlson, R.W., Nicklas, R.W., Yu, H.-M., Kang, J.-T., Li, C.-H., Huang, F. (2019) Vanadium isotope composition of the Bulk Silicate Earth: Constraints from peridotites and komatiites. *Geochimica et Cosmochimica Acta* 259, 288–301. https://doi.org/10.1016/j.gca.2019.06.008

Rasmussen, M.B., Halldórsson, S.A., Gibson, S.A., Guðfinnsson, G.H. (2020) Olivine chemistry reveals compositional source heterogeneities within a tilted mantle plume beneath Iceland. *Earth and Planetary Science Letters* 531, 116008. https://doi.org/10.1016/j.epsl.2019.116008

Schauble, E.A. (2004) Applying Stable Isotope Fractionation Theory to New Systems. *Reviews in Mineralogy and Geochemistry* 55, 65–111. https://doi.org/10.2138/gsrmg.55.1.65

Schuessler, J.A., Schoenberg, R., Sigmarsson, O. (2009) Iron and lithium isotope systematics of the Hekla volcano, Iceland — Evidence for Fe isotope fractionation during magma differentiation. *Chemical Geology* 258, 78–91. https://doi.org/10.1016/j.chemgeo.2008.06.021

Shi, J.-H., Zeng, G., Chen, L.-H., Hanyu, T., Wang, X.-J., Zhong, Y., Xie, L.-W., Xie, W.-L. (2022) An eclogitic component in the Pitcairn mantle plume: Evidence from olivine compositions and Fe isotopes of basalts. *Geochimica et Cosmochimica Acta* 318, 415–427. https://doi.org/10.1016/j.gca.2021.12.017

Shorttle, O., Maclennan, J. (2011) Compositional trends of Icelandic basalts: Implications for short–length scale lithological heterogeneity in mantle plumes. *Geochemistry, Geophysics, Geosystems* 12, Q11008. https://doi.org/10.1029/2011GC003748

Soderman, C.R., Matthews, S., Shorttle, O., Jackson, M.G., Ruttor, S., Nebel, O., Turner, S., Beier, C., Millet, M.-A., Widom, E., Humayun, M., Williams, H.M. (2021) Heavy δ^{57}Fe in ocean island basalts: A non-unique signature of processes and source lithologies in the mantle. *Geochimica et Cosmochimica Acta* 292, 309–332. https://doi.org/10.1016/j.gca.2020.09.033

Soderman, C.R., Shorttle, O., Matthews, S., Williams, H.M. (2022) Global trends in novel stable isotopes in basalts: Theory and observations. *Geochimica et Cosmochimica Acta* 318, 388–414. https://doi.org/10.1016/j.gca.2021.12.008

Sossi, P.A., O'Neill, H.St.C. (2017) The effect of bonding environment on iron isotope fractionation between minerals at high temperature. *Geochimica et Cosmochimica Acta* 196, 121–143. https://doi.org/10.1016/j.gca.2016.09.017

Sossi, P.A., Nebel, O., Foden, J. (2016) Iron isotope systematics in planetary reservoirs. *Earth and Planetary Science Letters* 452, 295–308. https://doi.org/10.1016/j.epsl.2016.07.032

Stow, M.A., Prytulak, J., Humphreys, M.C.S., Nowell, G.M. (2022) Integrated petrological and Fe-Zn isotopic modelling of plutonic differentiation. *Geochimica et Cosmochimica Acta* 320, 366–391. https://doi.org/10.1016/j.gca.2021.12.018

Williams, H.M., Bizimis, M. (2014) Iron isotope tracing of mantle heterogeneity within the source regions of oceanic basalts. *Earth and Planetary Science Letters* 404, 396–407. https://doi.org/10.1016/j.epsl.2014.07.033

Geochemical Perspectives Letters

No V-Fe-Zn isotopic variation in basalts from the 2021 Fagradalsfjall eruption

M.A. Stow, J. Prytulak, K.W. Burton, G.M. Nowell, E.W. Marshall, S.A. Halldórsson, S. Matthews, M.B. Rasmussen, E. Ranta, A. Caracciolo

Supplementary Information

The Supplementary Information includes:

1. Analytical Methods

Chemical purification and isotopic analysis were performed at the Arthur Holmes Isotope Geology Laboratory, Durham University.

Sample Digestion

Whole rock samples were ground into homogeneous powders by hand using an agate pestle and mortar, which was cleaned with low-Fe quartz sand between samples to avoid contamination. Approximately 30–50 mg of each powder was digested in 3 mL Teflon Distilled (TD) 29 M HF and 1 mL TD 16 M HNO_3 on a hotplate at 160 °C for 48 hours. Samples were evaporated at 120 °C to incipient dryness, then the residues were repeatedly covered with TD 16 M HNO_3 and evaporated at 180 °C until dark brown, indicating that insoluble fluorides were destroyed. Samples were dissolved in 1 mL TD 6 M HCl for the first column chromatography procedure.

Column Chromatography

The following column chromatography procedure quantitatively separates V, Fe and Zn from the same sample digestion. The first column follows the method of Sossi *et al.* (2015). Samples were loaded in 1 mL TD 6 M HCl onto Savillex

PFA columns containing 2 mL of pre-cleaned Bio-Rad AG1-X8 resin (200–400 mesh). The V fraction was collected as the samples were loaded, and with a further 4 mL TD 6 M HCl. Vanadium was eluted with most other matrix elements at this stage, and four further column chromatography procedures were required to fully purify the V fraction. The V fraction was evaporated and the residue was covered with TD 16 M HNO_3 and evaporated at 160 °C. This step was carried out twice between every column procedure to destroy any organic resin which may have passed through the frits.

After a 10 mL TD 6 M HCl wash, Fe was collected in 6 mL TD 0.5 M HCl and Zn was collected in 4 mL TD 3 M HNO_3. The Zn fraction was processed through the entire column procedure a second time. The Fe and Zn fractions were then evaporated and dissolved in 1 mL TD 3 % HNO_3 for isotopic analysis.

The procedure for further V separation is adapted from Nielsen *et al.* (2011) and Wu *et al.* (2016). The underlying principle is that V^{5+} forms anionic V-peroxide complexes with hydrogen peroxide (H_2O_2) in mildly acidic solutions, and these complexes will partition strongly onto AG1-X8 resin (Nielsen *et al.*, 2011). However, before H_2O_2 can be used, all Fe and Ti must be removed, because Fe and Ti can catalyse the dissociation of H_2O_2 to water and oxygen (Nielsen *et al.*, 2011). The first column procedure separates Fe, and the second column procedure, from Wu *et al.* (2016), removes Ti. The third column procedure, from Nielsen *et al.* (2011) then uses H_2O_2 and separates V from remaining matrix elements.

Column 2 (Wu *et al.*, 2016) uses 2 mL of pre-cleaned AG50W-X12 cation resin (200–400 mesh) in Savillex PFA columns. Samples were loaded in 1 mL 1 M HNO_3. 4 mL TD 1 M HNO_3 + 0.1 M HF was used to elute Ti and Al. The V fraction was then collected in 20 mL TD 1.2 M HNO_3.

Column 3 (Nielsen *et al.*, 2011) uses 1 mL of pre-cleaned AG1-X8 resin in quartz glass columns. Samples were dissolved in 1 mL 0.01 M HCl, and 33 µL H_2O_2 (1 % v/v) was added to cool samples immediately before loading, to form the V-peroxide complexes which partition onto the resin. Most matrix elements were eluted with 21 mL TD 0.01 M HCl + 1 % v/v H_2O_2 and V was then collected with 8 mL TD 1 M HCl.

The final two columns, from Nielsen *et al.* (2011) are small-scale clean-up columns designed to remove all remaining Ti and Cr from samples, because ^{50}Ti and ^{50}Cr are direct interferences on the minor ^{50}V isotope (Nielsen *et al.*, 2011). These columns were typically repeated twice each, with a Cr clean-up column always being the final column before isotopic analysis. For both procedures, Teflon micro-columns containing 100 µL AG1-X8 resin were used.

For the Ti clean-up column, samples were loaded in 1 mL TD 2 M HF. Vanadium was collected as the sample was loaded, and with a further 1.2 mL TD 2 M HF and 1.4 mL TD 0.5 M HF/HCl mixture. For the Cr clean-up column, which is a scaled down version of column 3, samples were dissolved in 1 mL TD 0.01 M HCl and 33 µL H_2O_2 was added to cool samples immediately before loading. After a wash of 0.6 mL TD 0.01 M HCl + 1 % H_2O_2, V was collected in 0.8 mL TD 1 M HCl. Samples were then re-dissolved in TD 3 % HNO_3 for isotopic analysis.

Isotope Ratio Measurements

All isotope ratio measurements were undertaken on Neptune or NeptunePlus MC-ICP-MS at Durham University. The USGS reference material BIR-1a was processed alongside unknowns, and gave Fe, V and Zn isotopic compositions which agree with previous measurements.

Vanadium. Vanadium isotope ratio measurements were made in medium resolution mode ($m/\Delta m \approx 6000$–8000), which allows V to be resolved from isobaric interferences. The sample introduction system consisted of a PFA concentric flow nebuliser (uptake rate 50 µL/min) coupled to an Aridus 2 desolvating nebuliser system, giving typical sensitivity of >100 V/ppm on ^{51}V. 2 mL sample aliquots were diluted with TD 3 % HNO_3 to a concentration of 1 µg/g V. Masses ^{48}Ti, ^{49}Ti, ^{50}V, ^{51}V, ^{52}Cr and ^{53}Cr were measured in Faraday cups L4, L2, L1, C, H1 and H3 respectively, with a 10^{10} Ω resistor connected to the centre cup to measure signals >50 V on ^{51}V. Standard sample bracketing with the AA standard (Nielsen *et al.*, 2011) was used to correct for mass bias. ^{48}Ti, ^{49}Ti, ^{52}Cr and ^{53}Cr were used to correct for interferences of ^{50}Ti and ^{50}Cr on ^{50}V, using the exponential law ($R_T = R_M \times (m_1/m_2)^{\beta}$ .Two BDH solutions (Nielsen *et al.*, 2011) were doped with 100 ppb Ti and Cr, respectively, and measured during every sequence. The β factor was then varied iteratively until δ^{51}V matched the long-term average BDH value of approximately −1.19 ‰ to −1.23 ‰ (Nielsen

et al., 2011; Wu *et al.*, 2016). These β factors were then used to correct for the interferences of ^{50}Ti and ^{50}Cr on all samples in the sequence, after Wu *et al.* (2016). USGS reference material BIR-1a gave a $\delta^{51}V_{AA}$ value of −0.87 ± 0.03 ‰ (2 s.d., n = 3).

Iron. Iron isotope ratio measurements were made in medium resolution mode ($m/\Delta m$ ≈ 6000–8000), which allows Fe to be resolved from isobaric oxide and nitride interferences. The sample introduction system consisted of a Savillex CF50 concentric flow nebuliser and ESI SIS spray chamber, giving a sensitivity of 5–8 V/ppm on ^{56}Fe. 2 mL sample aliquots were diluted with TD 3 % HNO_3 to a concentration of 10 µg/g Fe, and doped with 8 µg/g Ni. Masses ^{53}Cr, ^{54}Fe, ^{56}Fe, ^{57}Fe, ^{60}Ni and ^{61}Ni were measured on Faraday cups L4, L2, L1, C, H2 and H4. A 10^{10} Ω resistor was connected to L1 to measure signals of >50 V on ^{56}Fe. The isobaric interference of ^{54}Cr on ^{54}Fe was corrected by monitoring ^{53}Cr and assuming an exponential law. A combination of standard sample bracketing and external element doping with Ni was used to correct for mass bias (*e.g.*, Gong *et al.*, 2020). Samples were bracketed using the IRMM-524 standard, which is isotopically indistinguishable from IRMM-014 (Craddock and Dauphas, 2011). USGS reference material BIR-1a gave a $\delta^{56}Fe_{IRMM\text{-}524}$ value of 0.065 ± 0.043 ‰ (2 s.d., n = 6).

Zinc. Zinc isotope ratio measurements were made in low resolution mode ($m/\Delta m$ ≈ 400). The sample introduction system consisted of a Savillex CF50 concentric flow nebuliser and ESI SIS spray chamber, giving typical sensitivity of 6–7 V/ppm on ^{64}Zn. 2 mL sample aliquots were diluted with TD 3 % HNO_3 to a concentration of 750 ng/g Zn, and doped with 375 ng/g Cu. Masses ^{62}Ni, ^{63}Cu, ^{64}Zn, ^{65}Cu, ^{66}Zn, ^{67}Zn and ^{68}Zn were measured in Faraday cups L3, L2, L1, C, H1, H2, and H3, and 10^{11} Ω resistors were used on all cups. The isobaric interference of ^{64}Ni on ^{64}Zn was corrected by monitoring ^{62}Ni and assuming an exponential law. A combination of standard sample bracketing with the AA-ETH Zn solution (Archer *et al.*, 2017) and external element doping with Cu was used to correct for mass bias. Data in this study is reported relative to AA-ETH, which is offset relative to the commonly used reference standard JMC Lyon (Maréchal *et al.*, 1999) by +0.28 ± 0.02 ‰ (Archer *et al.*, 2017). This correction can be used to recast the data in this study relative to JMC-Lyon. USGS reference material BIR-1a gave a $\delta^{66}Zn_{AA\text{-}ETH}$ value of −0.033 ± 0.010 ‰ (2 s.d., n = 3), which is equivalent to a $\delta^{66}Zn_{JMC\text{-}Lyon}$ value of +0.247 ± 0.010 ‰ (2 s.d., n = 3).

2. Results

Table S-1 Vanadium, iron and zinc isotopic compositions of Fagradalsfjall lavas. Errors are given as 2 standard deviations of at least three measurements of an individual sample. Sample names and eruption day are from Halldórsson *et al.* (2022), where the eruption day is the best estimate of the day the material was erupted from the vent. The eruption day for sample G20210404-1 is unknown, but is between days 4 and 11. This sample is plotted as day 8 in all figures, which is the midpoint of this time period. Zinc isotopic compositions are expressed relative to the AA-ETH standard (Archer *et al.*, 2017). Data is recast relative to the JMC-Lyon standard using the correction of +0.28 ‰ (Archer *et al.*, 2017).

Sample Name	Eruption Day	$\delta^{51}V_{AA}$ (‰)	2 s.d.	*n*	$\delta^{56}Fe_{IRMM-524}$ (‰)	2 s.d.	$\delta^{57}Fe_{IRMM-524}$ (‰)	2 s.d.	*n*	$\delta^{66}Zn_{AA-ETH}$ (‰)	$\delta^{66}Zn_{JMC-Lyon}$ (‰)	2 s.d.	$\delta^{67}Zn_{AA-ETH}$ (‰)	2 s.d.	*n*
G20210321-2	2	−0.95	0.09	5	0.068	0.053	0.108	0.086	3	−0.027	0.253	0.021	−0.059	0.027	3
G20210323-1	4	−0.89	0.05	3	0.081	0.041	0.116	0.051	3	−0.028	0.252	0.036	−0.074	0.029	3
G20210330-2	11	−0.86	0.03	3	0.052	0.020	0.086	0.050	3	−0.026	0.254	0.003	−0.052	0.050	3
G20210404-1	4–11	−0.89	0.04	3	0.055	0.027	0.089	0.048	3	−0.012	0.268	0.017	+0.002	0.047	3
G20210405-1	17	−0.86	0.06	3	0.082	0.018	0.108	0.029	3	−0.019	0.261	0.009	−0.024	0.013	3
G20210412-1	24	−0.87	0.04	3	0.065	0.040	0.096	0.045	5	−0.020	0.260	0.013	−0.038	0.048	3
G20210412-2	24	−0.88	0.07	3	0.059	0.060	0.106	0.089	5	+0.013	0.293	0.027	−0.013	0.078	3
G20210416-3	28	−0.85	0.07	3	0.047	0.042	0.086	0.075	3	−0.037	0.243	0.024	−0.066	0.043	3
G20210416-4	25	−0.90	0.06	3	0.094	0.049	0.135	0.059	6	−0.042	0.238	0.003	−0.058	0.087	3
G20210424-5	36	−0.86	0.07	3	0.060	0.013	0.093	0.048	4	−0.023	0.257	0.031	−0.028	0.031	3
BIR-1a		−0.87	0.03	3	0.065	0.043	0.085	0.067	6	−0.033	0.247	0.010	−0.078	0.049	3

Table S-2 Compilation of data from Halldórsson *et al.* (2022) presented in this study.

Sample Name	Eruption Day	TiO_2 (wt. %)	K_2O (wt. %)	K_2O/TiO_2	La (µg/g)	Yb (µg/g)	La/Yb	$^{206}Pb/^{204}Pb$	2 s.e. (Abs)	$^{87}Sr/^{86}Sr$	2 s.e. (Abs)	$^{143}Nd/^{144}Nd$	2 s.e. (Abs)
G20210321-2	2	0.96	0.136	0.142	4.3	1.99	2.16			0.703109	0.000005	0.513010	0.000003
G20210323-1	4	0.97	0.144	0.148	4.3	1.96	2.20	18.7328	0.0012	0.703108	0.000008	0.513017	0.000003
G20210330-2	11	1.01	0.194	0.192	5.1	1.89	2.68	18.7567	0.0013	0.703125	0.000007	0.512991	0.000003
G20210404-1	4–11	1.03	0.213	0.208						0.703157	0.000005	0.512972	0.000004
G20210405-1	17	1.01	0.193	0.191	6.4	2.26	2.81	18.7607	0.0019	0.703139	0.000006	0.512984	0.000003
G20210412-1	24	1.08	0.259	0.241	8.0	2.13	3.76	18.8229	0.0014	0.703183	0.000006	0.512949	0.000004
G20210412-2	24	1.08	0.263	0.243									
G20210416-3	28	1.04	0.236	0.227	7.0	2.00	3.51						
G20210416-4	25	1.08	0.266	0.246	7.5	1.94	3.88						
G20210424-5	36	1.10	0.282	0.256	8.3	2.04	4.05	18.8389	0.0016				

3. Correcting Fe Isotopes for Fractional Crystallisation

Many studies correct the Fe isotopic composition of basalts for the effect of olivine crystallisation, in order to determine the Fe isotopic composition of the primary magma at the time of mantle melting ($\delta^{56}Fe_{prim}$).

The method, first presented in Sossi *et al*. (2016), is a mass balance calculation where olivine (with a composition in equilibrium with the current melt), is progressively added back into the melt until a Mg# of 0.74 is reached. This is assumed to reflect the composition of a primary mantle derived magma. The resulting change in the Fe isotopic composition of the melt is then also calculated by a mass balance calculation, assuming an appropriate $\Delta^{56}Fe_{ol\text{-}melt}$ value.

For the calculation, the FeO, MgO and $Fe^{3+}/\Sigma Fe$ of the uncorrected basalt must be known (or assumed), and used to calculate an initial Mg# (Mg# = $Mg^{2+}/(Mg^{2+} + Fe^{2+})$. The number of moles of Mg^{2+} and Fe^{2+} can be calculated using the atomic mass of MgO (40.3 amu) and FeO (71.8 amu) and the weight percent concentrations of MgO and FeO in the basalt (*i.e.* moles Mg^{2+} = MgO (wt. %)/40.3).

Following Sossi *et al*. (2016), for each 1 % incremental addition of olivine:

1) Calculate the composition of the olivine in equilibrium with the melt. We assume a Fe/Mg partition coefficient for olivine of 0.3 (Roeder and Emslie, 1970). Therefore, the Fe/Mg ratio of the olivine is given as:

$$\left(\frac{Fe}{Mg}\right)_{Ol} = K_{D\,Ol-melt}^{Fe-Mg} \times \left(\frac{Fe}{Mg}\right)_{melt}. \quad \text{(S-1)}$$

From olivine stoichiometry, we know that the number of moles of Fe + Mg must equal 2, which can be substituted into Equation S-1 to calculate the moles of Mg^{2+} and Fe^{2+} in the olivine. This can then be transformed into a concentration in wt. % using the atomic masses of the elements using Equations S-5 and S-7 as:

$$Fe^{2+} + Mg^{2+} = 2, \quad \text{(S-2)}$$

$$\left(\frac{Fe}{Mg}\right)_{Ol} = \frac{Mg^{2+} - 2}{Mg^{2+}}, \quad \text{(S-3)}$$

$$\text{moles } Mg^{2+} = \frac{2}{(1-(Fe/Mg)_{Ol})} \quad \text{and} \quad MgO_{Ol}\ (\text{wt. \%}) = \text{moles } Mg^{2+} \times 40.3, \quad \text{(S-4, S-5)}$$

$$Fe^{2+} = 2 - Mg^{2+} \quad \text{and} \quad FeO_{Ol}\ (\text{wt. \%}) = \text{moles } Fe^{2+} \times 71.8. \quad \text{(S-6, S-7)}$$

2) Calculate the new melt composition after olivine addition. For 1 % (0.01) incremental additions of olivine, this is given as:

$$FeO_{melt}^{new} = (1 - 0.01)FeO_{melt}^{previous} + (0.01)FeO_{Ol}, \quad \text{(S-8)}$$

$$MgO_{melt}^{new} = (1 - 0.01)MgO_{melt}^{previous} + (0.01)MgO_{Ol}. \quad \text{(S-9)}$$

3) Calculate the change in melt δ^{56}Fe following olivine addition. The proportion of Fe in olivine and melt is calculated as:

$$\Delta F(Fe) = (0.01) \times \frac{Fe_{Ol}}{Fe_{melt}}. \quad \text{(S-10)}$$

Then a mass balance equation is used to calculate the change in Fe isotopic composition of the melt:

$$\delta^{56}\mathrm{Fe_{Ol}} = \delta^{56}\mathrm{Fe_{melt}} + \Delta^{56}\mathrm{Fe_{Ol-melt}}, \quad \text{(S-11)}$$

$$\delta^{56}\mathrm{Fe_{melt}^{new}} = \big(1 - \Delta F(\mathrm{Fe})\big)\delta^{56}\mathrm{Fe_{melt}^{previous}} + \Delta F(\mathrm{Fe})\delta^{56}\mathrm{Fe_{Ol}}. \quad \text{(S-12)}$$

This is repeated incrementally until Mg# reaches 0.74 and olivine forsterite content reaches 90, which is assumed to represent a primary melt.

There are several different ways that $\Delta^{56}\mathrm{Fe_{Ol\text{-}melt}}$ can be calculated, which is a large source of uncertainty with the fractional crystallisation corrections. For this study, we used two separate methods:

- **Method 1:**

  From Sossi and O'Neill (2017), the olivine-melt fractionation factor can be expressed as:

  $$\Delta^{56}\mathrm{Fe_{Ol-melt}} = 2904 \times \frac{F_{\mathrm{Ol}} - F_{\mathrm{melt}}}{T^2}, \quad \text{(S-13)}$$

  where F_{Ol} has a value of 197 N/m (Dauphas *et al.*, 2014), F_{melt} varies depending on melt $\mathrm{Fe^{3+}/\Sigma Fe}$ but has a value of approximately 222 N/m when $\mathrm{Fe^{3+}/\Sigma Fe}$ is near 0.15 (since $F_{\mathrm{Fe^{2+}}}$ = 199 N/m and $F_{\mathrm{Fe^{3+}}}$ = 351 N/m; Dauphas *et al.*, 2014). Temperature is calculated using the expression from Nisbet (1982):

  $$T(\mathrm{K}) = [1000 + 20 \times \mathrm{MgO\ (wt.\%)}] + 273. \quad \text{(S-14)}$$

- **Method 2:**

  The maximum correction which has been proposed so far in the literature is $\Delta^{57}\mathrm{Fe_{Ol\text{-}melt}} = -0.4 \times 10^6/T^2$ (Nebel *et al.*, 2019) which is equivalent to $\Delta^{56}\mathrm{Fe_{Ol\text{-}melt}} = -0.276 \times 10^6/T^2$. We use this expression to calculate the maximum magnitude of possible fractional crystallisation correction.

For the Fagradalsfjall data, the corrected Fe isotopic compositions ($\delta^{56}\mathrm{Fe_{prim}}$) are shown in Figure S-1 by the red bars. Correction Method 1 gives a $\Delta^{56}\mathrm{Fe_{Ol\text{-}melt}}$ value of approximately −0.03 ‰, and a minimum δ^{56}Fe correction. We consider this to be a realistic correction because it is based on fractionation factors directly determined using NRIXS. Correction Method 2 gives a $\Delta^{56}\mathrm{Fe_{Ol\text{-}melt}}$ value of approximately −0.10 ‰, which we suspect may be an overcorrection of the data.

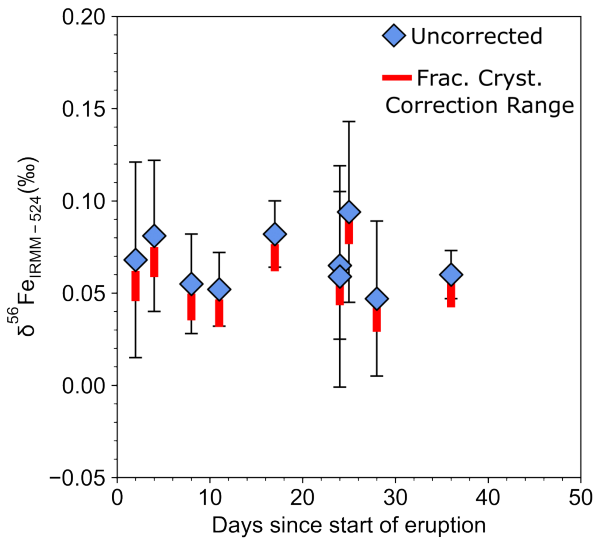

Figure S-1 Iron isotopic compositions of the Fagradalsfjall basalts corrected for olivine crystallisation. The red bar spans the range of the $\delta^{56}Fe_{prim}$ values calculated using two separate methods, as described in the text.

The Fagradalsfjall lavas are relatively primitive, with high Mg# between 64 and 67, and olivine cores with Fo content between 80 and 90 % (Halldórsson *et al.*, 2022), which suggests they have experienced limited fractional crystallisation. For both correction methods, the $\delta^{56}Fe_{prim}$ values are still within analytical uncertainty.

There are many uncertainties with fractional crystallisation corrections, the largest being which olivine-melt fractionation factors are selected. If different fractionation factors are chosen, discrepancies in the corrections are accentuated in those samples which have undergone the most olivine crystallisation. While this is less of an issue in the Fagradalsfjall samples, it becomes an increasingly important issue to consider in less primitive basalts, and those that crystallise phases other than olivine. In addition, there are uncertainties with assuming a $Fe^{3+}/\Sigma Fe$ for the melt, and in estimating accurate crystallisation temperatures.

For the above reasons, we chose to report and plot the uncorrected $\delta^{56}Fe$ values in this paper, as the correction had no effect on our Fe isotope trends or interpretations, and could instead increase uncertainty.

4. Fe Isotope Modelling During Mantle Melting

The variations in major and trace element composition in the Fagradalsfjall basalts is thought to be caused by changes in the proportions of melt contributed by depleted and enriched mantle domains over the course of the eruption, with melts from a geochemically enriched source becoming more significant with time (Halldórsson *et al.*, 2022). However, it is uncertain if this source is lithologically distinct (*i.e.* pyroxenitic). The aim of the Fe isotope modelling in this section is to investigate the source required to generate the trace element and Fe isotopic compositions of the Fagradalsfjall basalts.

We use a batch melting model after Sossi and O'Neill (2017) to model the trace element and Fe isotopic composition of melts produced from batch melting spinel lherzolite, garnet lherzolite, and pyroxenite sources (Fig. S-2). A full explanation of the calculations is given below. The parameters used are listed in Tables S-3 to S-6.

Batch Melting Models

Trace element concentrations in the melt (C_l) are calculated using a batch melting equation:

$$\frac{C_l}{C_o} = \frac{1}{(D+F(1-P))}. \qquad \text{(S-15)}$$

The Fe isotope modelling follows the approach outlined in Sossi and O'Neill (2017), and calculates the concentrations of the isotopes ^{54}Fe and ^{56}Fe in the melt (l). Equation S-16 is the general form of this equation, where i is the isotope being calculated, j denotes the normalising isotope (^{54}Fe), and C_o is the initial concentration in the bulk solid. F is the melt fraction, and is varied in steps of 0.02.

$$\frac{C_l^i}{C_o^i} = \frac{1}{\left(\left(D^j_{1-2}\alpha E^{\frac{i}{j}}_{1-2}\right)+F(1-P)\right)}. \qquad \text{(S-16)}$$

The term $\alpha E^{\frac{i}{j}}_{1-2}$ is the isotopic fractionation factor of element E, and is equivalent to the ratio of the two partition coefficients D^i_{1-2}/D^j_{1-2}. For example, Fe isotopes fractionation between the melt (l) and mantle (o) is expressed as:

$$\alpha \mathrm{Fe}^{\frac{56}{54}}_{l-o} = \frac{D^{56}_{l-o}}{D^{54}_{l-o}} = \frac{(^{56}\mathrm{Fe})_l\ /(^{56}\mathrm{Fe})_o}{(^{54}\mathrm{Fe})_l\ /(^{54}\mathrm{Fe})_o}. \qquad \text{(S-17)}$$

However, since at high temperatures, α is approximately equal to 1, the partition coefficients for D^j and D^i are approximately equal. It is assumed that the partition coefficient for the normalising isotope D^j (^{54}Fe) is equal to the bulk partition coefficient for Fe (see Sossi and O'Neill, 2017, for the full derivation). The partition coefficient for D^i (^{56}Fe) can then be calculated from Equation S-18, where K is the force constant of Fe-O bonds in the minerals and melt and x is a constant equal to 2904 which considers the difference in mass between the two isotopes (see Equation B-13 in Sossi and O'Neill, 2017, for the equation to calculate x):

$$D^{^{56}\mathrm{Fe}}_{min-melt} = \left(D^{^{54}\mathrm{Fe}}_{min-melt}\right) e^{\left(\frac{x\left(K^{min}_{Fe-O}-K^{melt}_{Fe-O}\right)}{T^2}\right)}. \qquad \text{(S-18)}$$

The force constants for the minerals are given in Tables S-4 to S-6, and remain constant throughout the model. We select force constants determined by the same method (NRIXS) for consistency. The force constant for the melt scales with melt $Fe^{3+}/\Sigma Fe$, and is calculated at each model step using Equation S-19, from the Dauphas *et al.* (2014) regression for force constants in basaltic, andesitic and dacitic glasses (a = 152 and b = 199):

$$K^{melt}_{Fe-O} = a \times \frac{Fe^{3+}}{\Sigma Fe} + b \qquad \text{(S-19)}$$

Therefore, for ^{56}Fe, Equation S-16 reduces to:

$$\frac{C_l^{56}}{C_o^{56}} = \frac{1}{\left(\left(D_{\text{min-melt}}^{56}\right)+F(1-P)\right)}, \qquad \text{(S-20)}$$

and for ^{54}Fe, Equation S-16 reduces to:

$$\frac{C_l^{54}}{C_o^{54}} = \frac{1}{\left(\left(D_{\text{min-melt}}^{54}\right)+F(1-P)\right)}. \qquad \text{(S-21)}$$

Dividing $\frac{C_l^{56}}{C_o^{56}}$ by $\frac{C_l^{54}}{C_o^{54}}$ gives the Fe isotope fractionation factor between the melt and the mantle ($\alpha Fe_{l-o}^{\frac{56}{54}}$; Eq. S-17). Therefore, the Fe isotopic composition of the melt can be calculated using Equation S-22, where $\delta^{56}Fe_o$ is the initial Fe isotopic composition of the mantle source.

$$\delta^{56}Fe_l = \delta^{56}Fe_o + 1000\ln\left(\frac{(^{56}Fe)_l\ /(^{56}Fe)_o}{(^{54}Fe)_l\ /(^{54}Fe)_o}\right) = \delta^{56}Fe_o + 1000\ln\left(\alpha Fe_{l-o}^{\frac{56}{54}}\right). \qquad \text{(S-22)}$$

Model Parameters

Table S-3 Initial Parameters for non-modal batch melting models for spinel peridotite, garnet peridotite and MORB-like pyroxenite.

Parameter	Spinel Peridotite	Reference	Garnet Peridotite	Reference	Pyroxenite	Reference
FeO (wt. %)	8.18	Workman and Hart (2005), DMM	8.18	Workman and Hart (2005), DMM	9.35	Lambart (2017), G2 pyroxenite
$Fe^{3+}/\Sigma Fe$	0.036	Sossi and O'Neill (2017), intermediate value	0.036	Sossi and O'Neill (2017), intermediate value	0.16	Cottrell and Kelley (2011), average MORB
$\delta^{56}Fe$	0.026	Craddock *et al.* (2013), DMM	0.026	Craddock *et al.* (2013), DMM	0.105	Teng *et al.* (2013), average MORB
La (µg/g)	0.192	Workman and Hart (2005), DMM	0.192	Workman and Hart (2005), DMM	2.695	Lambart (2017), G2 pyroxenite
Yb (µg/g)	0.365	Workman and Hart (2005), DMM	0.365	Workman and Hart (2005), DMM	3.4	Lambart (2017), G2 pyroxenite
Nb (µg/g)	0.1485	Workman and Hart (2005), DMM	0.1485	Workman and Hart (2005), DMM	6.13	Lambart (2017), G2 pyroxenite
Zr (µg/g)	5.082	Workman and Hart (2005), DMM	5.082	Workman and Hart (2005), DMM	65	Lambart (2017), G2 pyroxenite

Table S-4 Input parameters for melting a spinel-bearing depleted peridotite. Modal proportions are from Workman and Hart (2005). Melting coefficients are from Kinzler and Grove (1992). Partition coefficients for Fe^{2+} and Fe^{3+} are from Mallmann and O'Neill (2009). Trace element partition coefficients are from Gibson and Geist (2010). Force constants are from ([a]) Dauphas *et al.* (2014; forsterite value) and ([b]) Roskosz *et al.* (2015; median value for spinel). Due to the lack of NRIXS measurements for pyroxene, we assume olivine, orthopyroxene and clinopyroxene have equal force constants. In reality, Fe^{3+} bearing pyroxene will have a higher force constant than Fe^{2+} bearing olivine.

Mineral	Modal Proportion	Melting Coefficient	$D(Fe^{2+})$	$D(Fe^{3+})$	D(La)	D(Yb)	D(Nb)	D(Zr)	Force Constant (N/m)
olivine	0.57	−0.3	1.08	0.063	0.0005	0.02	0.0005	0.0033	197[a]
orthopyroxene	0.28	0.4	0.68	0.201	0.0031	0.08	0.004	0.013	197[a]
clinopyroxene	0.13	0.82	0.287	0.453	0.049	0.4	0.015	0.119	197[a]
spinel	0.02	0.08	1.93	2.88	0	0	0	0	264[b]

Table S-5 Input parameters for melting a garnet-bearing depleted peridotite. Modal proportions are from Hirschmann and Stolper (1996). Melting coefficients are from Walter (2003; garnet lherzolite at 3 GPa). Partition coefficients for Fe^{2+} and Fe^{3+} are from Mallmann and O'Neill (2009). Trace element partition coefficients are from Gibson and Geist (2010). The force constant for garnet is from Nie *et al.* (2021), and those for olivine and pyroxenes are as above.

Mineral	Modal Proportion	Melting Coefficient	$D(Fe^{2+})$	$D(Fe^{3+})$	D(La)	D(Yb)	D(Nb)	D(Zr)	Force Constant (N/m)
olivine	0.525	0.05	1.08	0.063	0.0005	0.02	0.0005	0.0033	197[a]
orthopyroxene	0.23	−0.15	0.68	0.201	0.0031	0.08	0.004	0.013	197[a]
clinopyroxene	0.175	0.96	0.287	0.453	0.049	0.4	0.015	0.119	197[a]
garnet	0.07	0.14	0.60	0.18	0.001	6.6	0.015	0.27	110

Table S-6 Input parameters for melting a MORB-like pyroxenite. Melting coefficients are from Pertermann and Hirschmann (2003). Modal proportions selected to represent an average pyroxenite. Partition coefficients for Fe^{2+} and Fe^{3+} for clinopyroxene are from Mallmann and O'Neill (2009), and assume that values are similar for garnet and orthopyroxene after Sossi and O'Neill (2017). Trace element partition coefficients are from Gibson and Geist (2010). The force constant for garnet is from Nie *et al.* (2021) and that for clinopyroxene is as above.

Mineral	Modal Proportion	Melting Coefficient	$D(Fe^{2+})$	$D(Fe^{3+})$	D(La)	D(Yb)	D(Nb)	D(Zr)	Force Constant (N/m)
clinopyroxene	0.8	0.872	0.287	0.453	0.049	0.4	0.015	0.119	197
garnet	0.2	0.173	0.60	0.18	0.001	6.6	0.015	0.27	110

Modelling Results

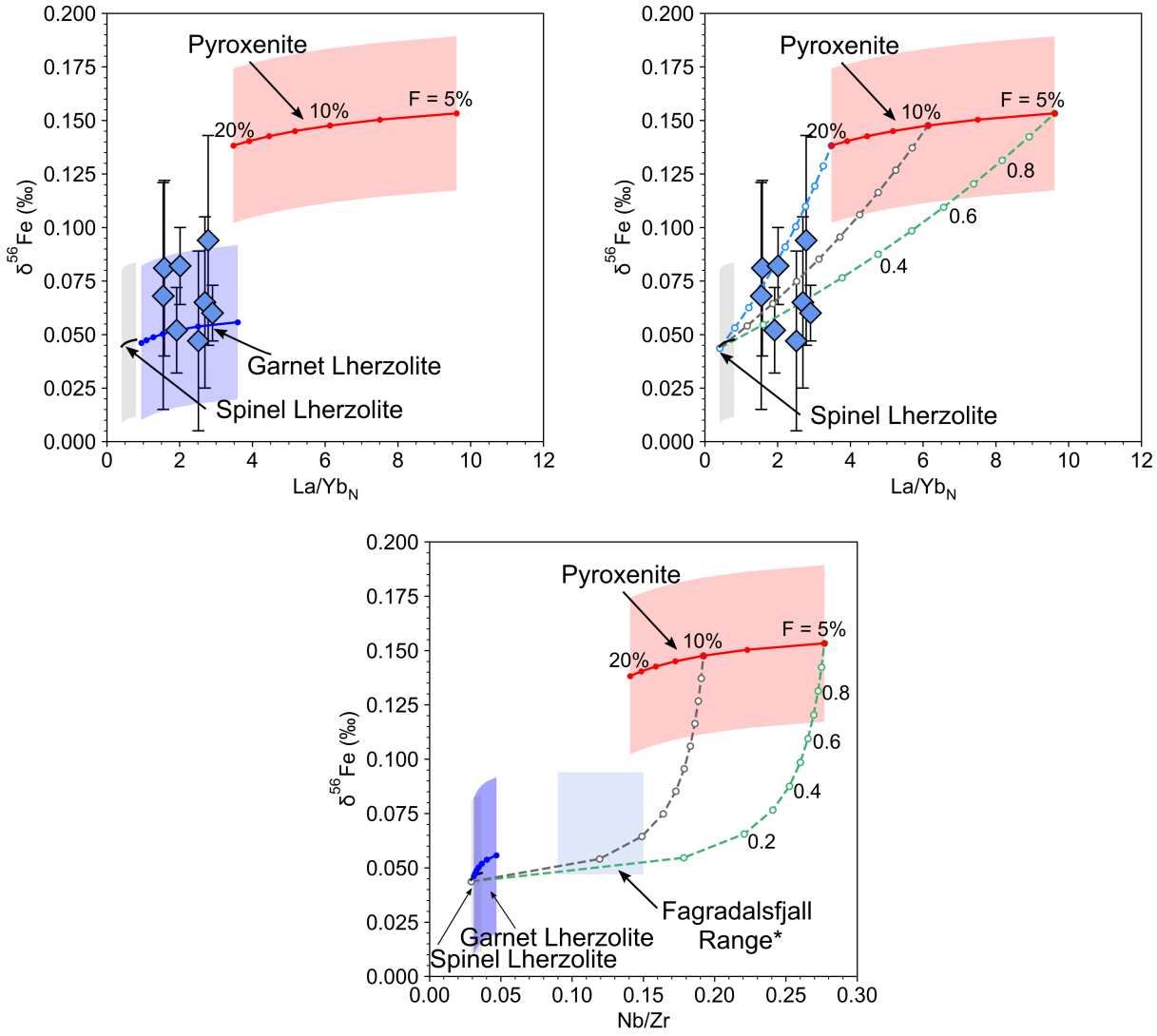

Figure S-2 Batch melting models of trace element and Fe isotopic composition, and binary mixing between end-member melts. La and Yb data are from Halldórsson *et al.* (2022). The Nb and Zr data for the Fagradalsfjall samples are for a different sample set from Bindeman *et al.* (2022), so are shown as a range.

Figure S-2 shows that if melting occurs within the spinel stability field, a minor proportion (~10–20 %) of pyroxenite melt is required to explain the La/Yb ratios of the lavas. However, if melting is >3 GPa and garnet is present in the mantle source, melting a garnet bearing peridotite at different pressures and melt fractions can explain the range of La/Yb and δ^{56}Fe in the Fagradalsfjall lavas. However, in order to explain the Nb/Zr ratios of the lavas (as reported in Bindeman *et al.*, 2022), a minor pyroxenite contribution (~10–20 % pyroxenite melt) is required. However, such a low proportion of pyroxenite does not cause resolvable variations in the major element or Fe isotopic composition of the melt.

In order to investigate the proportion and Fe isotopic composition of enriched end member melts which are required to cause a resolvable variation in basalt Fe isotopic composition, we construct a simple binary mixing model

using Equation S-23, where p is the proportion of end member A. For simplicity, the FeO content of the end member melts is assumed to be equal, although in reality this will vary with depth and degree of melting:

$$\delta^{56}Fe_{melt} = \frac{p*FeO_A*\delta^{56}Fe_A + (1-p)*FeO_B*\delta^{56}Fe_B}{p*FeO_A + (1-p)*FeO_B}. \quad \text{(S-23)}$$

Assuming a spinel lherzolite has initial δ^{56}Fe similar to the depleted MORB mantle (0.026 ‰; Craddock *et al.*, 2013), a depleted melt would have δ^{56}Fe ≈ 0.05 ‰ (*e.g.*, see Fig. S-2). For the enriched melt, if a pyroxenite source has initial δ^{56}Fe similar to average MORB (0.105 ‰; Teng *et al.*, 2013), the melt would have δ^{56}Fe ≈ 0.150 ‰ (*e.g.*, see Fig. S-2). However, pyroxenite xenoliths with δ^{56}Fe up to 0.20 ‰ have been measured previously (Zhao *et al.*, 2017). If the bulk melt-mantle fractionation factor is approximately 0.04–0.06 ‰ during pyroxenite melting, then a melt with δ^{56}Fe ≈ 0.25 ‰ could hypothetically be produced.

In reality, enriched melts are not sourced directly from the melting of subducted ocean crust. Instead, silica rich melts sourced from melting of recycled crust react with the peridotite mantle, consuming olivine and orthopyroxene and forming a hybrid source containing pyroxenite. Soderman *et al.* (2021) propose melts from reaction zone pyroxenites could be as heavy as δ^{57}Fe = 0.30 ‰ (or δ^{56}Fe ≈ 0.2 ‰), although these are likely rare heavy values. Therefore, we use a geologically feasible range of enriched end member compositions from 0.10 ‰ to 0.25 ‰.

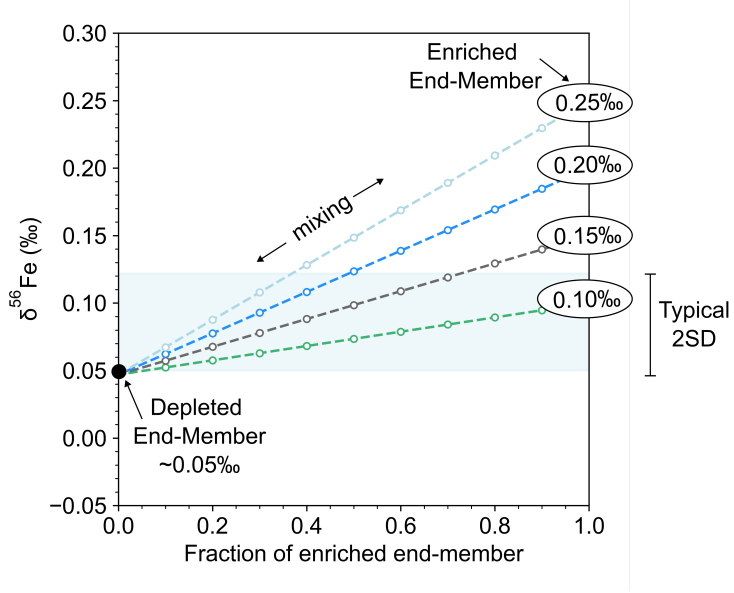

Figure S-3 Binary mixing model of depleted and enriched end members. The blue shaded area is the typical analytical uncertainty of Fe isotope measurements, which here is the average 2 s.d. measured in this study. Values for the depleted and enriched end members are discussed in the text.

The binary mixing model (Fig. S-3) shows that at current analytical uncertainty, at least 40–50 % enriched melt with δ^{56}Fe > 0.2 ‰ is generally required to generate resolvable Fe isotopic variation. This therefore suggests that at Fagradalsfjall there is no significant contribution of melts from a lithologically distinct (pyroxenite) mantle component, or the melting signal of enriched lithologies is masked by more significant peridotite melting.

Additional Figures

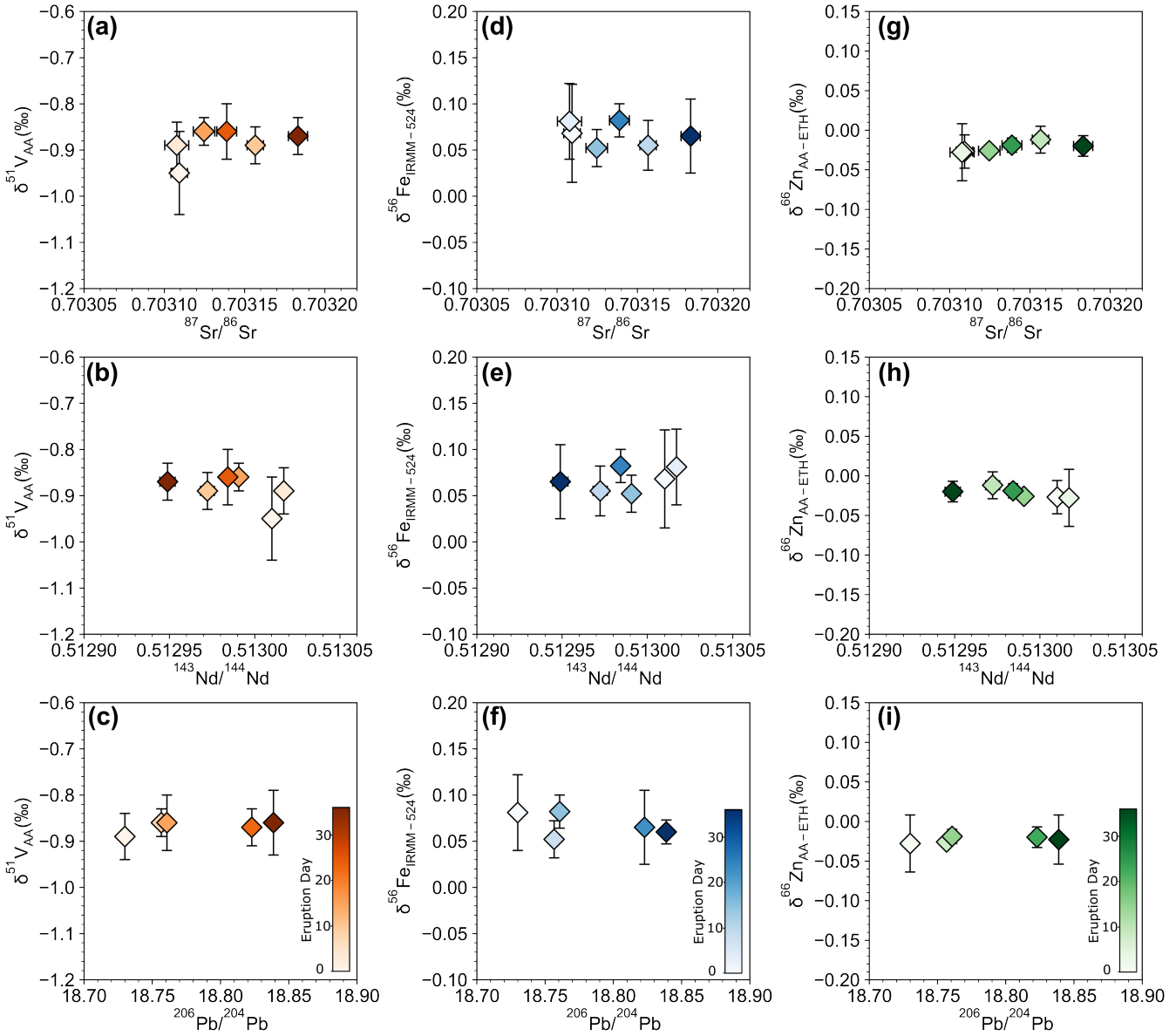

Figure S-4 Whole rock **(a–c)** vanadium, **(d–f)** iron and **(g–i)** zinc isotopic compositions plotted against **(a, d, g)** $^{87}Sr/^{86}Sr$, **(b, e, h)** $^{143}Nd/^{144}Nd$ and **(c, f, i)** $^{206}Pb/^{204}Pb$ from Halldórsson *et al.* (2022). The colour bars indicate the day the samples were erupted.

Supplementary Information References

Archer, C., Andersen, M.B., Cloquet, C., Conway, T.M., Dong, S., Ellwood, M., Moore, R., Nelson, J., Rehkämper, M., Rouxel, O., Samanta, M., Shin, K.-C., Sohrin, Y., Takano, S., Wasylenki, L. (2017) Inter-calibration of a proposed new primary reference standard AA-ETH Zn for zinc isotopic analysis. *Journal of Analytical Atomic Spectrometry* 32, 415–419. https://doi.org/10.1039/C6JA00282J

Bindeman, I.N., Deegan, F.M., Troll, V.R., Thordarson, T., Höskuldsson, Á., Moreland, W.M., Zorn, E.U., Shevchenko, A.V., Walter, T.R. (2022) Diverse mantle components with invariant oxygen isotopes in the 2021 Fagradalsfjall eruption, Iceland. *Nature Communications* 13, 3737. https://doi.org/10.1038/s41467-022-31348-7

Cottrell, E., Kelley, K.A. (2011) The oxidation state of Fe in MORB glasses and the oxygen fugacity of the upper mantle. *Earth and Planetary Science Letters* 305, 270–282. https://doi.org/10.1016/j.epsl.2011.03.014

Craddock, P.R., Dauphas, N. (2011) Iron Isotopic Compositions of Geological Reference Materials and Chondrites. *Geostandards and Geoanalytical Research* 35, 101–123. https://doi.org/10.1111/j.1751-908X.2010.00085.x

Craddock, P.R., Warren, J.M., Dauphas, N. (2013) Abyssal peridotites reveal the near-chondritic Fe isotopic composition of the Earth. *Earth and Planetary Science Letters* 365, 63–76. https://doi.org/10.1016/j.epsl.2013.01.011

Dauphas, N., Roskosz, M., Alp, E.E., Neuville, D.R., Hu, M.Y., Sio, C.K., Tissot, F.L.H., Zhao, J., Tissandier, L., Médard, E., Cordier, C. (2014) Magma redox and structural controls on iron isotope variations in Earth's mantle and crust. *Earth and Planetary Science Letters* 398, 127–140. https://doi.org/10.1016/j.epsl.2014.04.033

Gibson, S.A., Geist, D. (2010) Geochemical and geophysical estimates of lithological thickness variation beneath Galápagos. *Earth and Planetary Science Letters* 300, 275–286. https://doi.org/10.1016/j.epsl.2010.10.002

Gong, H., Guo, P., Chen, S., Duan, M., Sun, P., Wang, X., Niu, Y. (2020) A re-assessment of nickel-doping method in iron isotope analysis on rock samples using multi-collector inductively coupled plasma mass spectrometry. *Acta Geochimica* 39, 355–364. https://doi.org/10.1007/s11631-019-00392-4

Halldórsson, S.A., Marshall, E.W., Caracciolo, A., Matthews, S., Bali, E., Rasmussen, M.B., Ranta, E., Robin, J.G., Guðfinnsson, G.H., Sigmarsson, O., Maclennan, J., Jackson, M.G., Whitehouse, M.J., Jeon, H., van der Meer, Q.H.A., Mibei, G.K., Kalliokoski, M.H., Repczynska, M.M., Rúnarsdóttir, R.H., Sigurðsson, G., Pfeffer, M.A., Scott, S.W., Kjartansdóttir, R., Kleine, B.I., Oppenheimer, C., Aiuppa, A., Ilyinskaya, E., Bitetto, M., Giudice, G., Stefánsson, A. (2022) Rapid shifting of a deep magmatic source at Fagradalsfjall volcano, Iceland. *Nature* 609, 529–534. https://doi.org/10.1038/s41586-022-04981-x

Hirschmann, M.M., Stolper, E.M. (1996) A possible role for garnet pyroxenite in the origin of the "garnet signature" in MORB. *Contributions to Mineralogy and Petrology* 124, 185–208. https://doi.org/10.1007/s004100050184

Kinzler, R.J., Grove, T.L. (1992) Primary magmas of mid-ocean ridge basalts 1. Experiments and methods. *Journal of Geophysical Research: Solid Earth* 97, 6885–6906. https://doi.org/10.1029/91JB02840

Lambart, S. (2017) No direct contribution of recycled crust in Icelandic basalts. *Geochemical Perspectives Letters* 4, 7–12. https://doi.org/10.7185/geochemlet.1728

Mallmann, G., O'Neill, H.St.C. (2009) The Crystal/Melt Partitioning of V during Mantle Melting as a Function of Oxygen Fugacity Compared with some other Elements (Al, P, Ca, Sc, Ti, Cr, Fe, Ga, Y, Zr and Nb). *Journal of Petrology* 50, 1765–1794. https://doi.org/10.1093/petrology/egp053

Maréchal, C.N., Télouk, P., Albarède, F. (1999) Precise analysis of copper and zinc isotopic compositions by plasma-source mass spectrometry. *Chemical Geology* 156, 251–273. https://doi.org/10.1016/S0009-2541(98)00191-0

Nie, N.X., Dauphas, N., Alp, E.E., Zeng, H., Sio, C.K., Hu, J.Y., Chen, X., Aarons, S.M., Zhang, Z., Tian, H.-C., Wang, D., Prissel, K.B., Greer, J., Bi, W., Hu, M.Y., Zhao, J., Shahar, A., Roskosz, M., Teng, F.-Z., Krawczynski, M.J., Heck, P.R., Spear, F.S. (2021)

Iron, magnesium, and titanium isotopic fractionations between garnet, ilmenite, fayalite, biotite, and tourmaline: Results from NRIXS, *ab initio*, and study of mineral separates from the Moosilauke metapelite. *Geochimica et Cosmochimica Acta* 302, 18–45. https://doi.org/10.1016/j.gca.2021.03.014

Nielsen, S.G., Prytulak, J., Halliday, A.N. (2011) Determination of Precise and Accurate $^{51}V/^{50}V$ Isotope Ratios by MC-ICP-MS, Part 1: Chemical Separation of Vanadium and Mass Spectrometric Protocols. *Geostandards and Geoanalytical Research.* 35, 293–306. https://doi.org/10.1111/j.1751-908X.2011.00106.x

Nisbet, E.G. (1982). The tectonic setting and petrogenesis of komatiites. In: Arndt, N.T., Nisbet, E.G. (Eds.) *Komatiites*. Allen & Unwin, London, 501–520.

Nebel, O., Sossi, P.A., Bénard, A., Arculus, R.J., Yaxley, G.M., Woodhead, J.D., Davies, D.R., Ruttor, S. (2019) Reconciling petrological and isotopic mixing mechanisms in the Pitcairn mantle plume using stable Fe isotopes. *Earth and Planetary Science Letters* 521, 60–67. https://doi.org/10.1016/j.epsl.2019.05.037

Pertermann, M., Hirschmann, M.M. (2003) Anhydrous Partial Melting Experiments on MORB-like Eclogite: Phase Relations, Phase Compositions and Mineral-Melt Partitioning of Major Elements at 2–3 GPa. *Journal of Petrology* 44, 2173–2201. https://doi.org/10.1093/petrology/egg074

Roeder, P.L., Emslie, R.F. (1970) Olivine-liquid equilibrium. *Contributions to Mineralogy and Petrology* 29, 275–289. https://doi.org/10.1007/BF00371276

Roskosz, M., Sio, C.K.I., Dauphas, N., Bi, W., Tissot, F.L.H., Hu, M.Y., Zhao, J., Alp, E.E. (2015) Spinel-olivine-pyroxene equilibrium iron isotopic fractionation and applications to natural peridotites. *Geochimica et Cosmochimica Acta* 169, 184–199. https://doi.org/10.1016/j.gca.2015.07.035

Soderman, C.R., Matthews, S., Shorttle, O., Jackson, M.G., Ruttor, S., Nebel, O., Turner, S., Beier, C., Millet, M.-A., Widom, E., Humayun, M., Williams, H.M. (2021) Heavy $\delta^{57}Fe$ in ocean island basalts: A non-unique signature of processes and source lithologies in the mantle. *Geochimica et Cosmochimica Acta* 292, 309–332. https://doi.org/10.1016/j.gca.2020.09.033

Sossi, P.A., O'Neill, H.St.C. (2017) The effect of bonding environment on iron isotope fractionation between minerals at high temperature. *Geochimica et Cosmochimica Acta* 196, 121–143. https://doi.org/10.1016/j.gca.2016.09.017

Sossi, P.A., Halverson, G.P., Nebel, O., Eggins, S.M. (2015) Combined Separation of Cu, Fe and Zn from Rock Matrices and Improved Analytical Protocols for Stable Isotope Determination. *Geostandards and Geoanalytical Research* 39, 129–149. https://doi.org/10.1111/j.1751-908X.2014.00298.x

Sossi, P.A., Nebel, O., Foden, J. (2016) Iron isotope systematics in planetary reservoirs. *Earth and Planetary Science Letters* 452, 295–308. https://doi.org/10.1016/j.epsl.2016.07.032

Teng, F.-Z., Dauphas, N., Huang, S., Marty, B. (2013) Iron isotopic systematics of oceanic basalts. *Geochimica et Cosmochimica Acta* 107, 12–26. https://doi.org/10.1016/j.gca.2012.12.027

Walter, M.J. (2003) 2.08 - Melt Extraction and Compositional Variability in Mantle Lithosphere. In: Holland, H.D., Turekian, K.K. (Eds.) *Treatise on Geochemistry*. First Edition, Elsevier, Amsterdam, 363–394. https://doi.org/10.1016/B0-08-043751-6/02008-9

Workman, R.K., Hart, S.R. (2005) Major and trace element composition of the depleted MORB mantle (DMM). *Earth and Planetary Science Letters* 231, 53–72. https://doi.org/10.1016/j.epsl.2004.12.005

Wu, F., Qi, Y., Yu, H., Tian, S., Hou, Z., Huang, F. (2016) Vanadium isotope measurement by MC-ICP-MS. *Chemical Geology* 421, 17–25. https://doi.org/10.1016/j.chemgeo.2015.11.027

Zhao, X.M., Cao, H.H., Mi, X., Evans, N.J., Qi, Y.H., Huang, F., Zhang, H.F. (2017) Combined iron and magnesium isotope geochemistry of pyroxenite xenoliths from Hannuoba, North China Craton: implications for mantle metasomatism. *Contributions to Mineralogy and Petrology* 172, 40. https://doi.org/10.1007/s00410-017-1356-y